Annihilation Radiation of Dark Matter in Heterotic Orbifold Models

Gianfranco Bertone [1], Pierre Binétruy [2,3], Yann Mambrini [4], Emmanuel Nezri [2,3]

[1] *NASA/Fermilab Astrophysics Group, Fermi National*
Accelerator Laboratory, Box 500 Batavia, IL 60510-0500
[2] *Laboratoire de Physique Théorique des Hautes Energies,*
Université Paris-Sud, F-91405 Orsay
[3] *APC Université Paris 7, Collège de France, F-75231 Paris Cedex 05 and*
[4] *Departamento de Física Teórica C-XI and Instituto de Física Teórica C-XVI,*
Universidad Autónoma de Madrid, Cantoblanco, 28049 Madrid, Spain

Direct and indirect dark matter searches can potentially lead to the discovery of Supersymmetry. In the specific context of heterotic orbifold compactification scenarios, it is even possible to get some clues on the SUSY breaking mechanism of the more fundamental underlying theory. In this paper, we investigate the prospects for indirect detection of neutralino dark matter via gamma-ray (continuum and line) and synchrotron radiation from the Galactic center, in the context of AMSB scenarios in an effective heterotic framework, which constitutes a consistent SUSY model between high energy theory and low energy phenomenology.

I. INTRODUCTION

Many independent measurements provide convincing evidence that most of the matter in the Universe is dark, i.e. non–baryonic and of unknown nature, the most common dark matter (DM) candidate being a Weakly–Interacting Massive Particle (WIMP) [1]. Supersymmetric (SUSY) extensions of the Standard Model (SM) naturally predict a massive weakly interacting particle (WIMP) called neutralino ($\chi_1^0 \equiv \chi$), which, in most versions of SUSY models, is the lightest supersymmetric particle (LSP), and is made stable by virtue of the conservation of R–parity.

Dark matter searches are often discussed in the very popular mSUGRA, *a.k.a* CMSSM (constrained MSSM), model [2] where one assumes unification of the soft SUSY breaking parameters at the GUT scale. This assumption is essentially a reduction of the parameter space and has no real theoretical motivation. More refined SUSY models have been studied in the context of DM searches, relaxing the hypothesis of universality [3, 4, 5, 6, 7, 8, 9, 10, 11, 12, 13, 14, 15, 16].

Here we focus on effective string inspired models, which represent a possible consistent framework linking fundamental high energy theory with low energy physics. Recently, the full one loop soft supersymmetry breaking terms, in a large class of superstring effective theories, have been calculated [17], based on orbifold compactifications of the weakly–coupled heterotic string (including the so–called anomaly mediated contributions). The parameter space in this class of models has already been severely constrained taking into account accelerator and relic density constraints [18], direct or indirect detection of DM from the Sun [19], or benchmark models at the Tevatron [20]. In this model, supersymmetry breaking is transmitted by the auxiliary ('F') fields of the compactification moduli T^α, whose expectation values determine the size of the compact manifold, or by the dilaton auxiliary field S, whose vacuum expectation value determines the magnitude of the coupling constant $g_{\rm STR}$. The spectrum and couplings of SUSY particles depend crucially on the contributions of each hidden fields to the breaking mechanism.

There exist many ways of probing the existence of neutralino dark matter and supersymmetry. Of course, accelerator searches are among the most promising ones. Recent results give a mass limit of 45 GeV for the lightest neutralino, in the framework of mSUGRA [25]. Furthermore, interesting constraints have been derived from many experiments on direct and indirect detection of dark matter, whose sensitivities are expected to increase by orders of magnitude in the near future (see Ref. [1] and references therein). Direct detection is made via the measurement of the recoil energy of the nuclei of the detector after an elastic scattering with a WIMP. Indirect detection experiments look for the products of annihilation of the LSP in the Sun, Galactic halo or external galaxies (see Ref. [1] and references therein).

It has been emphasized in [19] that one–ton detectors are needed for direct searches to test all the parameter space in scenarios dominated by the dilaton $F-$breaking terms, and that moduli dominated scenarios are generically not detectable by dark matter searches (direct or indirect detection with neutrinos coming from the Sun) if we combine favored relic density and accelerator constraints. This means that such DM searches could be a way to distinguish the origin(s) of the SUSY breaking mechanism, and to restrict or even determine some fundamental parameters of the model (of stringy nature or not).

The purpose of the present paper is to investigate DM indirect detection with high energy gamma rays and synchrotron radiation from neutralino annihilation at the Galactic center, in the class of weakly coupled heterotic string models discussed above [17, 18, 19, 20].

The paper is organized as follows: after a brief survey on the motivations, phenomenology and construction of the effective string models studied here, we analyze in section 2 and 3 the influence of the different coefficients parameterizing the SUSY breaking, on the gamma-ray and synchrotron emission from the Galactic center. In section 4, we analyze the prospects of observation of gamma-ray fluxes with present and foreseen experiments and discuss synchrotron radiation in section 5. We present our conclusions in section 6.

II.   THEORETICAL FRAMEWORK

A.   Structure of heterotic orbifolds models at one loop

The task of string phenomenology is to make contact between the high energy string theory, and the low energy world. For this purpose, we need to build a superstring theory in four dimensions, able to reproduce the Standard Model gauge group, three generations of squarks, and a coherent mechanism of SUSY breaking. We set our analysis in the framework of orbifold compactifications of the heterotic string, within the context of supergravity effective theory, we focus on models where the action is dominated by 1–loop contributions to soft breaking terms. The key property of the models is the non–universality of soft terms, consequences of the beta–function appearing in the superconformal anomalies. This non–universality gives a peculiar phenomenology in the gaugino and the scalar sector, modifying considerably the predictions of mSUGRA models. In fact, these string–motivated models show a new behavior, that interpolates between the phenomenology of unified supergravity models (mSUGRA) and models dominated by the superconformal anomalies (AMSB). The constraints arising from accelerator searches, and some dark matter aspects (direct and neutrino indirect detections) have been already studied in [18, 19]. We extend here the analysis to gamma-ray and synchrotron emission from the Galactic center.

We provide a phenomenological study within the context of orbifold compactifications of the weakly–coupled heterotic string, where we distinguish two regimes:

- In the first one, the SUSY breaking is transmitted by the compactification moduli T^α, whose vacuum expectation values determine the size of the compact manifold. Generic (0,2) orbifold

models contain three T_α moduli fields. We considered a situation in which only an "overall modulus T" field contributes to the SUSY–breaking. The use of an overall modulus T is equivalent to the assumption that the three T_α fields of generic orbifold models give similar contributions to SUSY–breaking. This is expected in the absence of some dynamical effect that would strongly discriminate the three moduli.

• In the second case, it is the dilaton field S present in any four–dimensional string (whose vacuum expectation value determine the magnitude of the unified coupling constant $g_{\rm STR}$ at the string scale), that transmits, via its auxiliary component, the SUSY breaking. We work in the context of models in which string nonperturbative corrections to the Kähler potential act to stabilize the dilaton in the presence of gaugino condensation [21, 22].

The origin of the soft breaking terms are completely different in the two scenarios. Some are coming from the superconformal anomalies and are non–universal (proportional to the beta–function of the Standard Model gauge groups), others are generated in the hidden sector (from Green–Schwarz mechanism or gaugino condensation) and are thus universal. This mixture between universality and non–universality gives the richness of the phenomenology in this type of effective string models and confirms the interest of non–universal studies in the prospect of supersymmetric dark matter detection, non–universality being in this case connected with the basic properties of the model.

B.   SUSY parameters and constraints

In all the models considered here, the lightest neutralino is the LSP. Its phenomenology (mainly the couplings and the spectrum) is determined by its mass matrix,

$$
\mathcal{M}_N = \begin{pmatrix} M_1 & 0 & -m_Z \cos\beta \sin\theta_W & m_Z \sin\beta \sin\theta_W \\ 0 & M_2 & m_Z \cos\beta \cos\theta_W & -m_Z \sin\beta \cos\theta_W \\ -m_Z \cos\beta \sin\theta_W & m_Z \cos\beta \cos\theta_W & 0 & -\mu \\ m_Z \sin\beta \sin\theta_W & -m_Z \sin\beta \cos\theta_W & -\mu & 0 \end{pmatrix} . \tag{1}
$$

written in the $(\tilde{B}, \tilde{W}^3, \tilde{H}_d^0, \tilde{H}_u^0)$ basis, where, $\tilde{B}$, $\tilde{W}^3$, $\tilde{H}_d^0$, $\tilde{H}_u^0$ represents respectively the B–ino, W–ino and down, up–Higgsinos fields. M_1, M_2 and μ are the bino, wino, and Higgs–Higgsino mass parameters respectively. Tanβ is the ratio of the *vev* of the two Higgs doublet fields. This matrix can be diagonalized by a single unitary matrix z such that we can express the LSP as

$$
\chi = z_{\chi 1}\tilde{B} + z_{\chi 2}\tilde{W} + z_{\chi 3}\tilde{H}_1 + z_{\chi 4}\tilde{H}_2. \tag{2}
$$

The parameter μ is obtained under the requirement that the electroweak symmetry breaking (EWSB) takes place. This is done by computing the complete one–loop corrected effective potential. The effective μ–term is calculated from the EWSB condition after minimization of the scalar potential

$$
\mu^2 = \frac{\left(m_{H_d}^2 + \delta m_{H_d}^2\right) - \left(m_{H_u}^2 + \delta m_{H_u}^2\right)\tan^2\beta}{\tan^2\beta - 1} - \frac{1}{2}M_Z^2 \tag{3}
$$

The sign of μ is not determined and left as free parameter.

We clearly see that the nature of the neutralino (and its couplings) depends crucially on the hierarchy between the parameters M_1, M_2 and μ.

C. The moduli dominated scenario

In the moduli dominated scenario, the one loop order supersymmetric SUSY breaking terms at GUT scale can be written [17, 23, 24]:

$$M_a = \frac{g_a^2(\mu)}{2} \left\{ 2 \left[\frac{\delta_{\text{GS}}}{16\pi^2} + b_a \right] G_2(T,\overline{T})F^T + \frac{2}{3} b_a \overline{M} \right\}, \tag{4}$$

$$A_{ijk} = -\frac{1}{3}\gamma_i \overline{M} - p\gamma_i G_2(T,\overline{T})F^T + \text{cyclic}(ijk), \tag{5}$$

$$M_i^2 = (1-p)\gamma_i \frac{|M|^2}{9}. \tag{6}$$

where M_a and M_i are the soft masses for the gauginos and scalars and A_i, the trilinear coupling. b_a is the beta–function coefficient for the gauge group G_a:

$$b_a = \frac{1}{16\pi^2} \left(3C_a - \sum_i C_a^i \right). \tag{7}$$

where C_a, C_a^i are the quadratic Casimir operators for the group G_a in the adjoint representation and in the representation of the field i respectively. F^S and F^T are the auxiliary fields for the dilaton and the Kähler modulus, respectively, $\overline{M}$ is the supergravity auxiliary fields whose vacuum expectation value (vev) determines the gravitino mass $m_{3/2} = -\frac{1}{3}\overline{M}$, and δ_{GS} is the Green–Schwarz coefficient which is a (negative) integer between 0 and -90. The function $G_2(T,\overline{T})$ is proportional to the Eisenstein function and vanishes when T is stabilized at one of its two self–dual points. From Eq.(4), it follows that when the moduli are stabilized at a self dual point, only the second term contributes to gaugino masses. This is precisely the "anomaly mediated" contribution. The loop contributions have been computed using the Pauli–Villars (PV) regularization procedure. The PV regular fields mimic the heavy string modes that regulate the full string amplitude. The phenomenological parameter p which represents the effective modular weight of the PV fields is constrained to be not larger than 1, though it can be negative in value. Thus the scalar squared mass for all matter fields is in general non–zero and positive at one loop (only the Higgs can have a negative running squared mass). The limiting case of $p = 1$, where the scalar masses are zero at one loop level and for which we recover a sequestered sector limit, occurs when the regulating PV fields and the mass–generating PV fields have the same dependance on the Kähler moduli. Another reasonable possibility is that the PV masses are independent of the moduli, in which case we would have $p = 0$. and γ_i is related to the anomalous dimension through $\gamma_i^j = \gamma_i \delta_i^j$. (see [17, 18, 20] for notations and conventions)

We clearly see in these formulae the competition between universal terms and non–universal ones. The scalar mass terms are all non–universal and proportional to their anomalous dimension and thus loop suppressed. The Green-Schwarz mechanism generates universal breaking terms for the gauginos (proportional to δ_{GS}) whereas superconformal anomalies introduce non–universal contributions (proportional to b_a). The nature of the neutralino thus depends mainly on the value of the Green–Schwarz counterterm δ_{GS}, whereas the mass scale is the gravitino mass $m_{3/2}$. We illustrate in Figs.1 the neutralino mass and its relic density as a function of δ_{GS}, vertical directions correspond to different values of $m_{3/2}$.
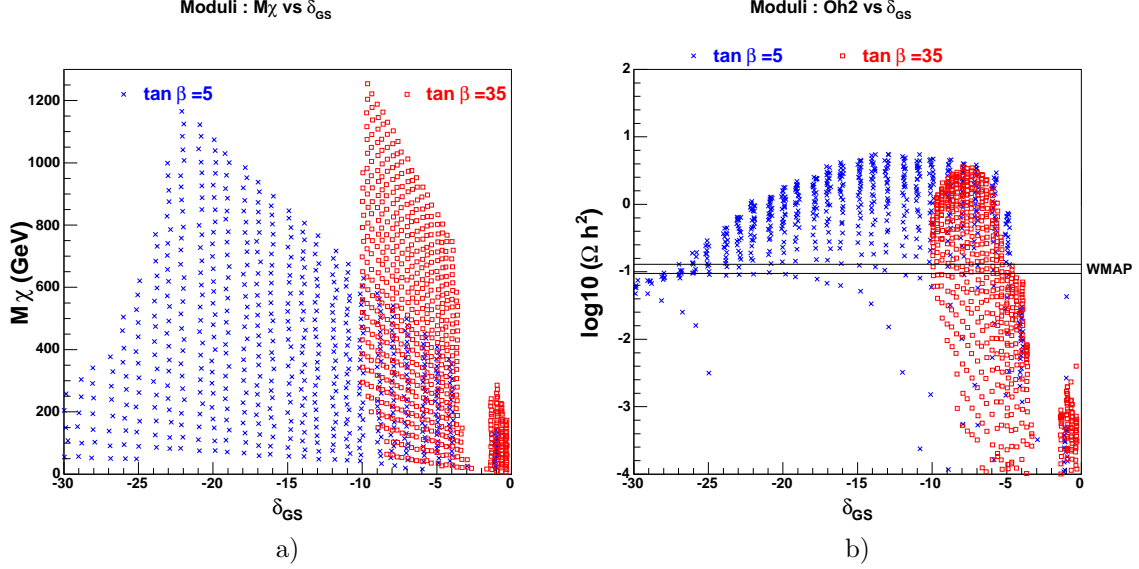
FIG. 1: a) Neutralino mass b) Relic density as a function of δ_{GS} for $t = 0.25$, $p = 0$, $\tan\beta = 5$ in blue crosses (resp. 35 in red boxes) and $0 < m_{3/2} < 10$ (resp. 20) TeV. The hole for small $|\delta_{GS}|$ values corresponds to a gluino LSP corridor and the left boundary of the clouds corresponds to the stau LSP region (see Figs.4 and 12)

D. The dilaton dominated scenario

We turn now to a scenario where the dilaton is the primary source of supersymmetry breaking in the observable sector. It is well known that if we use the standard Kähler potential derived from the tree level string theory, it is very difficult to stabilize the dilaton at acceptable weak–coupling values. We postulate, in our study, nonperturbative correction of stringy origin to the dilaton Kähler potential. In that case, one condensate can stabilize the dilaton at weak coupling, while simultaneously ensuring vanishing expectation values at the minimum of the potential. The key feature of such models is the deviation of the dilaton Kähler metric from its tree level value. If we imagine the superpotential for the dilaton having the form $W(S) \propto e^{-3S/b_+}$, with b_+ being the largest beta–function coefficient among the condensing gauge groups of the hidden sector, then we are led to consider the phenomenology of models given by the following pattern of soft supersymmetry breaking terms [17, 23, 24]:

$$M_a = \frac{g_a^2(\mu)}{2}\left\{\frac{2}{3}b_a\overline{M} + \left[1 - 2b_a'K_s\right]F^S\right\} \tag{8}$$

$$A_{ijk} = -\frac{K_s}{3}F^S - \frac{1}{3}\gamma_i\overline{M} + \tilde{\gamma}_iF^S\left\{\ln(\mu_{\mathrm{PV}}^2/\mu_R^2) - p\ln\left[(t+\bar{t})|\eta(t)|^4\right]\right\} + (ijk) \tag{9}$$

$$M_i^2 = \frac{|M|^2}{9}\left[1 + \gamma_i - \left(\sum_a \gamma_i^a - 2\sum_{jk}\gamma_i^{jk}\right)\left(\ln(\mu_{\mathrm{PV}}^2/\mu_R^2) - p\ln\left[(t+\bar{t})|\eta(t)|^4\right]\right)\right]$$
$$+ \left\{\tilde{\gamma}\frac{MF^S}{6} + \mathrm{h.c.}\right\}, \tag{10}$$

where μ_{UV} is an ultraviolet regularization scale (of the order of the string scale M_{STR}) and μ_R the renormalization scale (taken at the boundary value of M_{GUT})[56]. Moreover

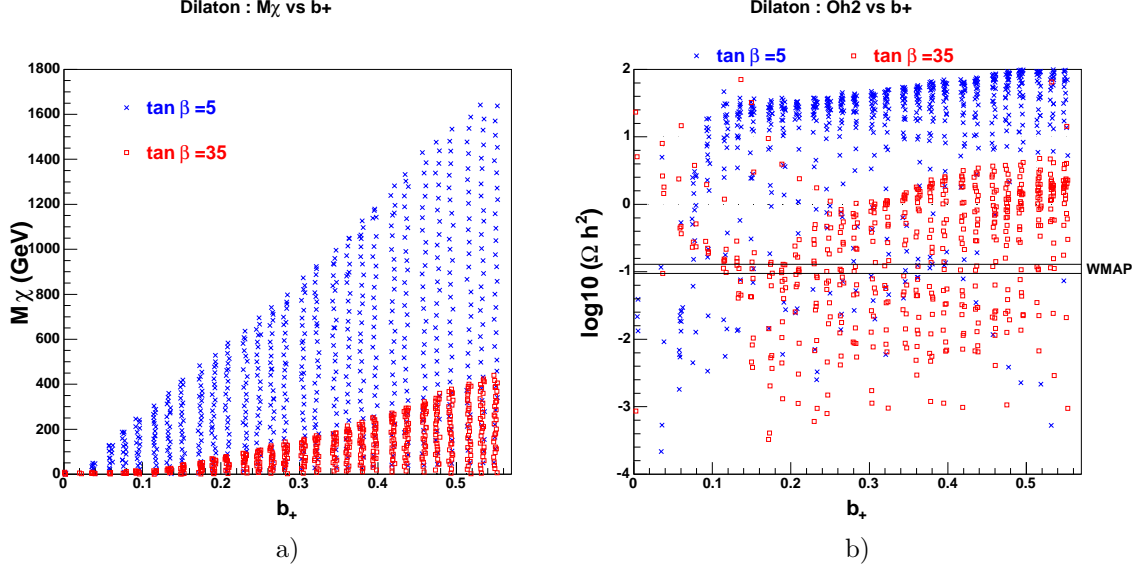**Dilaton : Mχ vs b+**

Dilaton : Oh2 vs b+

a)

b)

FIG. 2: a) Neutralino mass b) Relic density as a function of b_+ for $t = 0.25$, $p = 0$, $\tan\beta = 5$ in blue crosses (resp. 35 in red boxes) and $0 < m_{3/2} < 15$ (resp. 4) TeV.

$$F^S = \sqrt{3}m_{3/2}(K_{s\bar{s}})^{-1/2}, \quad K_{s\bar{s}} = \partial_s\partial_{\bar{s}}K, \tag{11}$$

and

$$(K^{s\bar{s}})^{-1/2} = \sqrt{3}\frac{\frac{2}{3}b_+}{1 - \frac{2}{3}b_+K_s}, \quad K_s = -g_{STR}^2/2. \tag{12}$$

(see [17, 18, 20] for notations and conventions) to ensure a vanishing vacuum energy in the dilaton–dominated limit.

The phenomenology of a dilaton–dominated scenario is completely different from a moduli–dominated one. If we look at formulae (8) and (10), it is clear that we are in a domain of heavy squarks and sleptons (of the order of magnitude of the gravitino mass) and relatively light gauginos. Indeed, the factor b_+, as it contains a loop factor, can suppress the magnitude of the auxiliary field F^S relative to that of the supergravity auxiliary field M through the relation (11). The resulting gaugino soft breaking terms are less universal for low values of b_+. We illustrate neutralino mass and relic density as a function of b_+ in Figs.2.

III.   SUPERSYMMETRIC DARK MATTER PHENOMENOLOGY

A.   Relic density

The relic density of neutralinos depends on their composition. In a large parameter space of the mSUGRA model, the bino–like nature of the lightest neutralino χ implies a rather low rate of annihilation.

Different processes lead to interesting neutralino relic density. Let us begin with a brief survey. For a bino neutralino one needs sfermion coannihilation or annihilation into the pseudo-scalar A to

have a cosmologically favoured abundance of neutralino. If the lightest neutralino has a dominant wino component the relic density drops because of efficient annihilations into gauge bosons as well as strong $\chi\chi_1^+$ coannihilations. For a non negligible higgsino component, the neutralino annihilates into gauge bosons or $t\bar{t}$ and relic density is also decreased by $\chi\chi_1^+$ and $\chi\chi_2^0$ coannihilations.

In Fig.1 (resp. 2), decreasing δ_{GS} (resp. b_+) in the moduli (resp. dilaton) dominated scenario corresponds to going from a dominant wino (resp. bino) to a dominant bino (resp. higgsino) component. The theoretically predicted relic density can be checked against cosmological observations. In particular, recent data on the cosmological microwave background (CMB) from the WMAP satellite [26] constrain the dark matter relic density to be (at the 2σ level) in the range $\Omega_{\rm CDM}h^2 = 0.1126^{+0.0161}_{-0.0181}$. We indicate on Figs 1b) and 2b) the WMAP favoured range, keeping in mind that the relic density calculation is very sensitive to SUSY mass and coupling uncertainties. In the following, we plot models in a generous range of relic density $0.03 < \Omega h^2 < 0.3$, indicating also the WMAP constraint.

B. Dark matter profiles

A crucial ingredient for the calculation of annihilation fluxes is the density profile of dark matter, which is usually parameterized as

$$\rho(r) = \frac{\rho_0}{(r/R)^\gamma [1 + (r/R)^\alpha]^{(\beta-\gamma)/\alpha}} \quad . \tag{13}$$

where r is the galacto-centric coordinate, R is a characteristic length and α, β and γ are free parameters. Unfortunately, large uncertainties are associated with such profiles, especially in the innermost regions of galaxies, i.e. regions where, in many cases, most of the signal comes from.

N-body simulations suggest the existence of 'cuspy' profiles, following a power law $\rho(r) = r^{-\gamma}$ where γ should be ~ 1 at small radii, although its exact value is under debate. Several groups tried to reproduce the initial results of Navarro, Frenk & White [27], who found $\gamma = 1$, but reached different conclusions. In Tab. I we give the values of the parameters (α, β, γ) for some of the most widely used profile models, namely the Kravtsov et al. (Kra, [28]), Navarro, Frenk and White (NFW, [27]), Moore et al. (Moore, [29]) and modified isothermal (Iso, e.g. [30]) profiles. The most recent N-body simulations (Hayashi et al 2003) suggest that profiles do not approach power laws with a well defined index at very small radii. Profiles continue to become shallower, i.e. the (negative) logarithmic slope becomes higher, when moving towards the centre.

Furthermore, the presence of a 3.6×10^6 solar masses black hole lying at the Galactic Center (see e.g.Ref. [31]) could possibly modify the profile of dark matter, that would accrete on it producing a so-called 'spike' [32], leading to an enhancement of the annihilation flux by several orders of magnitude. The prospects of indirect detection of dark matter in presence of such a spike have been discussed in Ref. [33] (see ibid. for a discussion of the dynamical effects, recently proposed in literature, that could potentially destroy the spike). The observational situation is even more unclear. Density profiles are usually reconstructed from the observation of rotation curves of galaxies, in particular of low surface brightness galaxies (LSB), that are thought to be dark matter dominated. de Blok et al. [34] used this method to claim the inconsistency of the observed 'flat' profiles, with the cuspy profiles predicted by n-body simulations. Other groups [35, 36] claimed instead that cuspy profiles are compatible with observations. Hayashi et al [37] compared the observational data with their numerical simulations (not with fitting formulae of their simulations) and found no significant discrepancy in most cases. They attributed the remaining discrepancies to the difference between circular velocities and gas rotation speed in realistic triaxial halos. For more information on DM profiles see Ref. [1]. We assume in the following a NFW profile, and an

	α	β	γ	R (kpc)	$\bar{J}\left(10^{-3}\right)$
Kra	2.0	3.0	0.4	10.0	2.166×10^{1}
NFW	1.0	3.0	1.0	20	1.352×10^{3}
Moore	1.5	3.0	1.5	28.0	1.544×10^{5}
Iso	2.0	2.0	0	3.5	2.868×10^{1}

TABLE I: Parameters of some widely used density profiles models and corresponding value of $\bar{J}(10^{-3})$.

observation angle of 10^{-3} sd, the results for other profiles can be easily obtained using the numbers in Tab.1.

C. Flux of secondary particles

Indirect detection of dark matter is based on the observation of secondary particles originating from dark matter annihilations in a cosmic storage area like the galactic halo. The study presented here is conceptually similar to the one in Ref. [38], devoted to indirect detection of Kaluza-Klein dark matter.

The observed flux of secondary particle of species i, from the annihilation of dark matter particles of mass M and annihilation cross section σv, from a direction ψ and at energy E, can be expressed as (e.g. Ref. [38, 39])

$$\Phi_i(\psi, E) = \sigma v \frac{dN_i}{dE} \frac{1}{4\pi M^2} \int_{\text{line of sight}} d\,s\rho^2\left(r(s,\psi)\right) \qquad (14)$$

where dN_i/dE is the spectrum of secondary particles per annihilation and $r^2 = s^2 + R_0^2 - 2lR_0 \cos\psi$, with $R_0 \sim 8.5$kpc is the solar distance to the galactic center.

It is customary (see [30]), in order to separate the factors depending on astrophysics from those depending only on particle physics, to introduce the quantity $J(\psi)$

$$J(\psi) = \frac{1}{8.5\,\text{kpc}} \left(\frac{1}{0.3\,\text{GeV/cm}^3}\right)^2 \int_{\text{line of sight}} d\,s\rho^2\left(r(s,\psi)\right) . \qquad (15)$$

We then define $\bar{J}(\Delta\Omega)$ as the average of $J(\psi)$ over a spherical region of solid angle $\Delta\Omega$, centered on $\psi = 0$. The values of $\bar{J}(\Delta\Omega = 10^{-3})$ are shown in the last column of Tab. I for the corresponding density profiles. In what follows, we assume a NFW profile : results corresponding to the other profiles of Table 1) can be deduced by a rescaling of $\bar{J}$

WIMP annihilation in the Galactic Halo produce a flux of gamma–rays, with either a continuum (coming from π^0 decay after the shower from hadronization of the neutralino annihilation products (quarks or gauge/higgs bosons)) or a monochromatic distribution (produced from one–loop annihilation into $\gamma\gamma$ or $Z\gamma$). Monochromatic processes are loop suppressed, and contribute little to the γ spectrum. But, as the neutralino can be considered at rest, the monochromatic ray is at an energy equal to the neutralino mass. This could be one of the most promising signals for the discovery of supersymmetry in dark matter searches.

At the same time, annihilating neutralinos can also generate positron fluxes. Cosmic–ray electrons and positrons interact with the interstellar medium through synchrotron radiation and inverse Compton scattering. The observed $e^{\pm}$ flux is dominated by primary electrons from acceleration

sites, however, 10 percent of the total flux is made of secondary electrons and positrons produced (in equal number) by the interaction of the primaries with the interstellar medium.

Data from $HEAT$ (High Energy Antimatter Telescope) suggest the existence of a "bump" in the positron flux around 10 GeV [40]. Halos of neutralinos could be a new source of positron explaining this excess, as there is no standard mechanism that would produce a signal at such a high energy. However, it is difficult to reproduce the normalization of the observed positron fraction even assuming that fluxes are "boosted", e.g. because of the presence of dense DM substructures in the solar neighborhood (see the discussion and references in Ref. [1]). Moreover, these secondary $e^\pm$ could propagate in the galactic magnetic field, generating synchrotron radiation (see below).

D. Experiments

Up to now, detectors have explored energy ranges above ~ 300 GeV (ground–based telescopes like Whipple or Cangaroo) or below ~ 20 GeV (EGRET). But the region which might turn to be the most promising one for neutralino physics is the intermediate region (30 GeV $< E_\gamma <$ 300 GeV) that will be explored by the next generation of detectors. In this paper we focus on the complementarity of two type of telescope : a ground–based Atmospheric Čerenkov Telescope (*High Energy Stereoscopic System*, HESS) and a satellite experiment (*Gamma–Ray Large Area Space Telescope*, GLAST).

Ground–based and satellite experiments are complementary sources of data for supersymmetric dark matter searches. While satellite experiments allow for a lower energy threshold (less than 1 GeV for GLAST), a better energy resolution and a longer exposure time, the small effective area of the order of the square meter limits the sensitivity to high energy photons. On the contrary, the large effective areas (~ 0.1 km^2 for HESS) of ground-based Cerenkov telescopes permit the measurement of very high energy fluxes with a higher energy threshold ($E_\gamma > 60$ GeV for HESS)

IV. ANALYSIS

Gamma ray fluxes strongly depend on the phenomenology of the neutralino. On the other hand, the nature of the neutralino is determined by the fundamental parameters of the models at high scale. We first analyze the dependence of neutralino annihilation on the main parameters of moduli dominated scenario ($m_{3/2}$, δ_{GS}, $\tan\beta$) or dilaton dominated scenario ($m_{3/2}$, b_+) and then the resulting gamma flux dependence on these parameters. We then compare the predictions of our models with the sensitivities of present and future gamma ray experiments. All calculations are achieved assuming an intermediate NFW profile: the results for other distributions can be easily deduced from a rescaling by using the $\bar{J}$ values in the table I.

A. Neutralino annihilation

The main neutralino annihilation processes are $\chi\chi \overset{Z}{\rightarrow} t\bar{t}$ ($\sigma_{t\bar{t}} \propto [z^2_{\chi 3(4)}]^2$), $\chi\chi \overset{\chi^+}{\rightarrow} W^+W^-$ ($\sigma_{WW} \propto [z_{\chi 3(4)} V_{12}]^2$ and/or $[z_{\chi 2} V_{11}]^2$ where $V_{11(2)}$ is the wino (higgsino) component of the exchanged chargino) and $\chi\chi \overset{A}{\rightarrow} b\bar{b}$ ($\sigma_{b\bar{b}} \propto [z_{\chi 1(2)} z_{\chi 3(4)}]^2$). Thus, both neutralino wino and higgsino components strongly enhance annihilation. The processes are shown in Figs. 3. The opening of the different channels obviously depends on kinematics (m_χ versus m_b, m_W, m_t). For a dominant bino LSP ($M_1 << M_2, \mu$), the s–channel A exchange (Fig. 3d) is the only one present. This process is dominating for low m_A especially when m_χ approaches $m_A/2$ (A–pole) and is thus favored for high
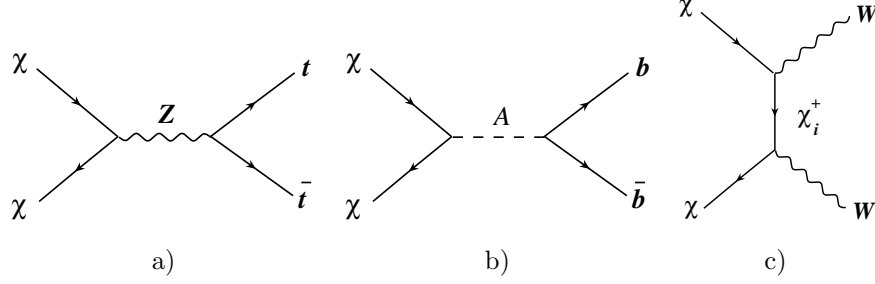
FIG. 3: **The dominant Feynman graph** contributing for the process $\chi \chi \to \gamma \gamma$.

values of $\tan \beta$ thanks to the $b\overline{b}$ coupling to the pseudoscalar. When kinematically allowed, annihilation into $t\overline{t}$ final state by Z exchange can be also open despite the coupling suppression. For a wino–like neutralino ($M_2 << M_1$, μ), the annihilation into WW final state through χ_1^+ exchange (Fig. 3c) is dominant thanks to the $\chi\chi_1^+ W$ coupling *and* its propagator factor ($m_\chi \sim M_2 \sim m_{\chi^+}$). For an higgsino–like neutralino ($\mu << M_1$, M_2), when $m_\chi > m_t$, the Z exchange ($t\overline{t}$ final state) is enhanced through the $\chi\chi Z$ coupling. But for even lower values of μ (*i.e* neutralino mass), $t\overline{t}$ final state is kinematically closed, and the neutralinos self annihilate into W^+W^- or $b\overline{b}$ (when $m_\chi < m_W$) final states.

The differential energy spectrum of the photon depends a lot on the primary product of the neutralino annihilation. The gamma–ray spectrum was simulated in [54] and fitted well with the function $dN_\gamma/dx = ae^{-bx}/x^{1.5}$, where $x = E_\gamma/m_\chi$ and $(a,b) = (0.73, 7.76)$ for WW and ZZ, $(1.0, 10.7)$ for $b\overline{b}$, $(1.1, 15.1)$ for $t\overline{t}$, and $(0.95, 6.5)$ for $u\overline{u}$. As we will see later on, final states with gauge boson will produce the harder spectrum.

B. Gamma-ray flux in the moduli dominated scenario

The integrated gamma flux gives a good understanding of the phenomenological aspects of the moduli sector of the theory.

As an illustration, dominant annihilation branching ratios are represented as a function of δ_{GS} and $m_{3/2}$ in Figs. 4 for $\tan \beta = 35$ (and in appendix Figs. 12 for $\tan \beta = 5$) without any experimental cut on the parameter space. We also show in Fig. 5a the integrated (from 1GeV to m_χ) gamma flux for a NFW halo profile as a function of the Green–Schwarz counterterm δ_{GS} for two values of $\tan\beta$ (5,35) and $m_{3/2} = 10$ TeV. To complete our illustration, we have plotted in Fig. 5b the mass spectrum $2m_\chi$ and M_A for the same set of parameters. The mass of the neutralino (increasing with $|\delta_{GS}|$, Eq. 4) and its nature (from wino to bino with increasing $|\delta_{GS}|$) determine in a large part the integrated flux. Indeed the LSP is mainly bino–like for $-20 < \delta_{GS} < -3$ and wino–like[57] for $-3 < \delta_{GS} < 0$.

Fig. 5a illustrates first the general increase of the flux as a function of δ_{GS}, due to the decrease of the neutralino mass (Fig. 5b). For δ_{GS} running from -10 to -4, we observe a higher flux for higher $\tan\beta$ because the A–pole channel is kinematically open for $\delta_{GS} \sim -5$ at $\tan \beta = 35$ (value of δ_{GS} that gives $2m_\chi > M_A$). This process produces a large amount of $b\overline{b}$ final states (Fig. 4) thanks to the coupling $Ab\overline{b}$, proportional to $\tan\beta$. The low $\tan\beta$ (Fig. 12) dominant channel is the $t\overline{t}$, proportional to $\frac{m_t m_\chi}{m_Z^2}$. For $-2 < \delta_{GS} < 0$, the neutralino is entirely *wino*, leading to annihilation into WW (Fig. 4). Indeed, a crude approximation tell us that the WW cross section is proportional to $z_{\chi 2}^4 (\sim 1$ for $\delta_{GS} = -1)$ and the annihilation into $t\overline{t}$, proportional to the square of the $\chi\chi Z$ coupling ($\left[z_{\chi 3}^2 + z_{\chi 4}^2 \right]^2 \sim 10^{-5}$ for $\delta_{GS} = -4$.). This explains the 5 orders of magnitude
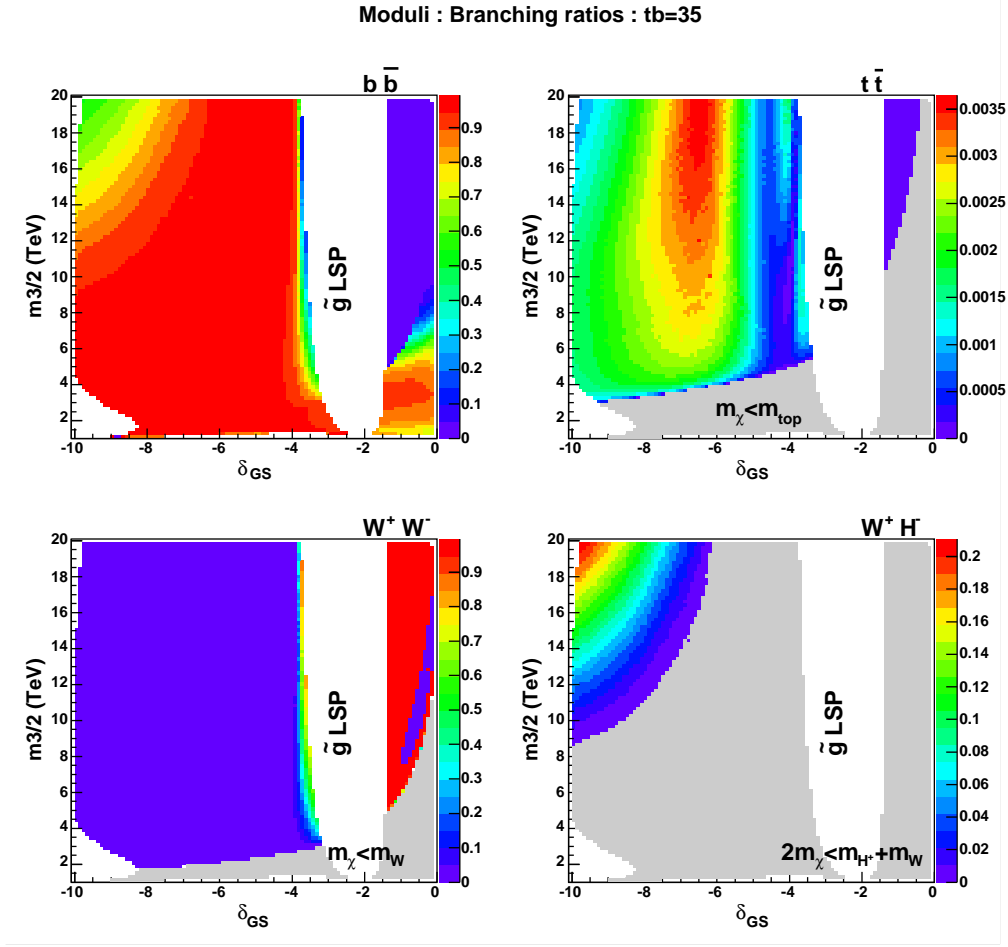
FIG. 4: Moduli domination regime: dominant annihilation branching ratios in the $(\delta_{GS}, m_{3/2})$ plane for $\tan\beta = 35$, $t = 0.25$, $p = 0$. Regions with gluino LSP are indicated. We also show in grey the kinematically forbidden region for each channel.

observed on the Fig. 5 between the small and large values of $|\delta_{GS}|$ for $\tan\beta = 35$.

For $\delta_{GS} \sim 0$ and small values of $m_{3/2}$, when the WW channel is kinematically closed, dominant γ–ray contribution comes from the annihilation into $b\bar{b}$ through Z and A exchange (suppressed because proportional to m_b). For $\tan\beta = 5$ and for higher $m_{3/2}$ values one can have $t\bar{t}$ or gg annihilation channels which explains the change of slope of the flux with $\tan\beta = 5$ on Fig. 5.

C. Gamma-ray flux in the dilaton dominated scenario

In scenarios where the supersymmetry is spontaneously broken through the *vev* of the dilaton auxiliary field, the β function b_+ of the first gaugino condensing group plays a role similar to the Green–Schwarz counterterm $|\delta_{GS}|$ in the moduli domination scenario. Since b_+ does not depend on the gauge group indices of the Standard Model $SU(3) \times SU(2) \times U(1)$, it contributes universally to the gaugino mass breaking terms. Thus, the phenomenology of dilaton scenarios at large b_+ in the gaugino sector is similar to the one of the moduli dominated models at large $|\delta_{GS}|$. The scalar sector is responsible of most of the phenomenological differences. Indeed, the scalar masses are non–universal and suppressed in moduli like scenario because of the loop anomaly factors suppression
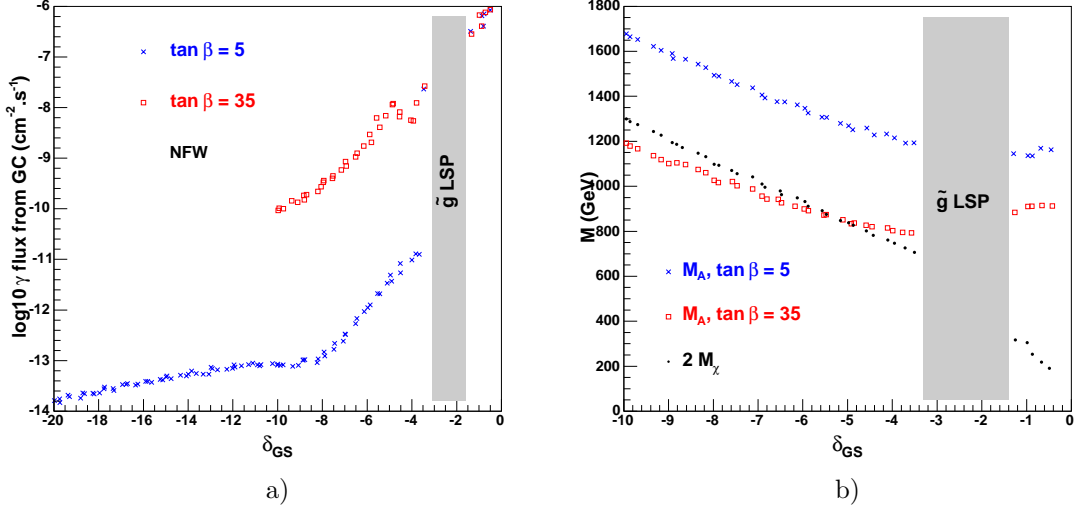
FIG. 5: Moduli-dominated scenario. a) The integrated gamma flux ($E_\gamma > 1$ GeV) for a NFW profile in the moduli parameter space as a function of the Green Schwarz counterterm δ_{GS}, for $m_{3/2} = 10$ TeV, $t = 0.25$, $p = 0$, $\tan \beta = 5$ (blue crosses) and 35 (red boxes) and b) the relevant mass spectrum of as a function of δ_{GS} for the same values of $\tan \beta$. See the text for the comments.

$\gamma_i \sim \frac{1}{16\pi^2}$ (Eq. 6), whereas they are universal and large in a dilaton dominated scenario ($m_0 \sim m_{3/2}$ Eq. 10). The main consequences are heavier pseudoscalar[58] A and $M_{H_u}^2$ breaking term at GUT scale, that drives the μ parameter to lower values, especially in high $\tan\beta$ regimes, Eq.(3).

As in the moduli dominated scenario, we show the dominant annihilation branching ratios, in the ($b_+, m_{3/2},$) plane for $\tan \beta = 35$ in Figs.6 (and in appendix in Figs.13 for $\tan \beta = 5$) to highlight the different annihilation channel dependence on fundamental parameter. We also show (in Fig. 7a) the integrated gamma flux for a threshold $E_\gamma > 1$ GeV, from the Galactic Center for a NFW profile, as a function of b_+, for two values of $\tan\beta$ (5 and 35) and the higgsino fraction of the lightest neutralino in Fig. 7b.

The effect of b_+ on the neutralino nature is complex and indirect. It acts on M_3 through the F^S contribution with a different sign contribution than the superconformal contribution proportional to b_3 (Eq. (8). Thus, lowering b_+ acts through the M_3 dependence of the RGE on $M_{H_u}^2$. Lower b_+ means lower M_3, Eq.(8) leading to higher $M_{H_u}^2$ through the RGE implying a lower μ parameter, Eq.(3): neutralino is mainly higgsino for $b_+ < 0.1(0.3)$ and $\tan\beta=5$ (35) as we can see in Fig. 7b. Though quite low, its wino component is not completely negligible.

For a fixed value of $m_{3/2}$, decreasing b_+ lead to a higher higgsino fraction favoring WW, ZZ channels and the $t\bar{t}$ one when kinematically open (*i.e* for high $m_{3/2}$ values) compared to the $b\bar{b}$ channel. For low $m_{3/2}$ values the wino component also favors the WW channel. When $m_\chi < m_W$, annihilation into $b\bar{b}$ is completely dominant, the other processes being kinematically closed. This is illustrated on Figs. 6 for $\tan \beta = 35$ and in appendix Fig. 13 for $\tan \beta = 5$. For a given $m_{3/2}$, higher values of $\tan\beta$ give better fluxes because it enhances the higgsino fraction of the neutralino through Eq.(3). The neutralino mass increasing with b_+ (Fig.2a) explains the general evolution of the gamma flux ($\propto \frac{1}{m_\chi^2} \sim \frac{1}{M_1^2}$) (Fig. 7a). The gamma flux follows also the higgsino fraction (Fig. 7b) which enhances the annihilation. The different peaks correspond to changes in hierarchy between M_1, μ, M_W in the neutralino mass matrix Eq. 1 exchanging the annihilation processes (Fig. 6). The different flux slopes (Fig.7) correspond to the different spectrum shape of each
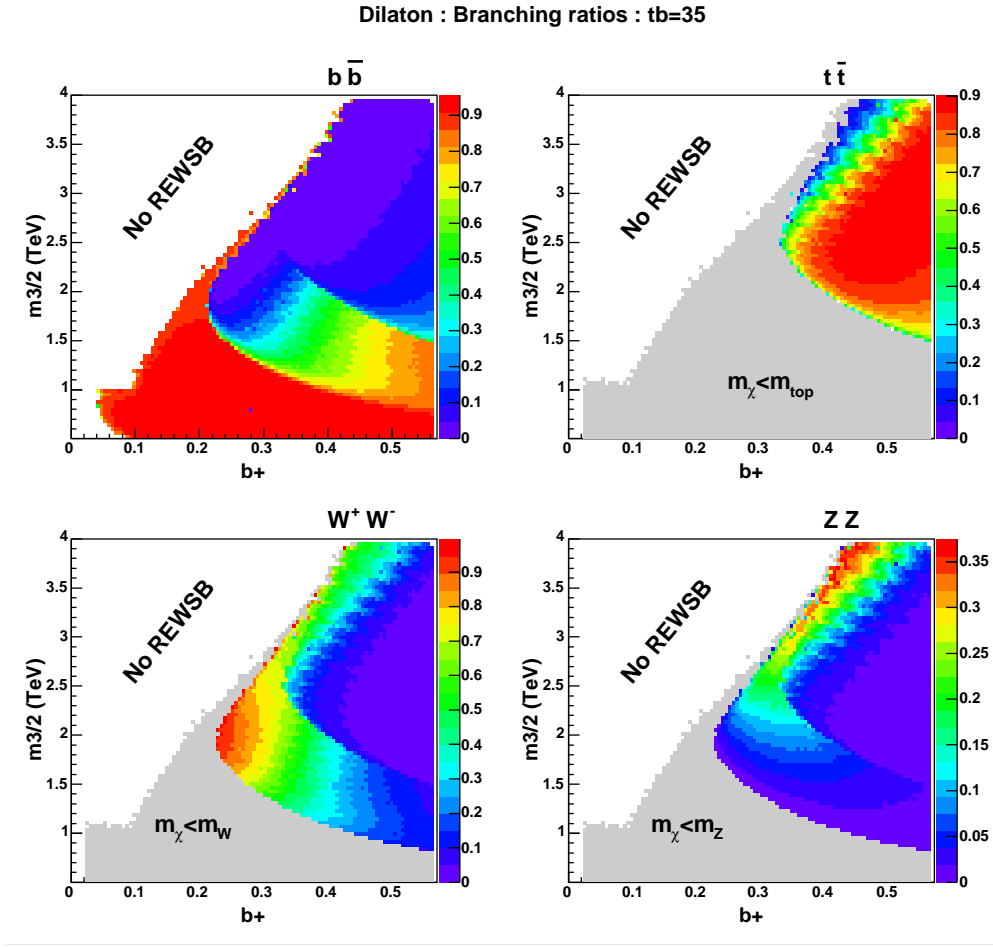
Dilaton : Branching ratios : tb=35

FIG. 6: Dilaton domination regime: dominant annihilation branching ratios in the $(b_+, m_{3/2})$ plane for $\tan\beta = 35$, $t = 0.25$, $p = 0$. Regions where radiative electroweak symmetry breaking can not occur are indicated (No REWSB). We also show in grey the kinematically forbidden region for each channel.

neutralino annihilation final states (Fig.6).

D. Comparison of models in view of the experimental sensitivities

The phenomenology of the two SUSY breaking mediation sectors strongly depends on the fundamental parameter space of the models at GUT scale. It is then interesting to look back at the prospect of discovering gamma fluxes as a function of a physical parameter, the neutralino mass (m_χ), and to compare both SUSY breaking scenarios with mSUGRA. For that purpose, we have computed the total gamma flux as a function of m_χ for three values of $\tan\beta$, scanning on the two other main parameters of each model ($[m_{3/2}, \delta_{GS}]$ in the moduli dominated case and $[m_{3/2}, b_+]$ in the dilaton dominated one). We have applied the experimental cuts coming from LEPII constraints on SUSY spectrum, higher order processes and neutralino relic density favored regions (the details are developed in appendix C).

We have first plotted in Figs 8a and 9a the total gamma flux coming from the Galactic Center above 1 GeV as a function of the neutralino mass for a NFW profile and different values of $\tan\beta$ (5, 20, 35) in the moduli and dilaton dominated scenarios. We note that:
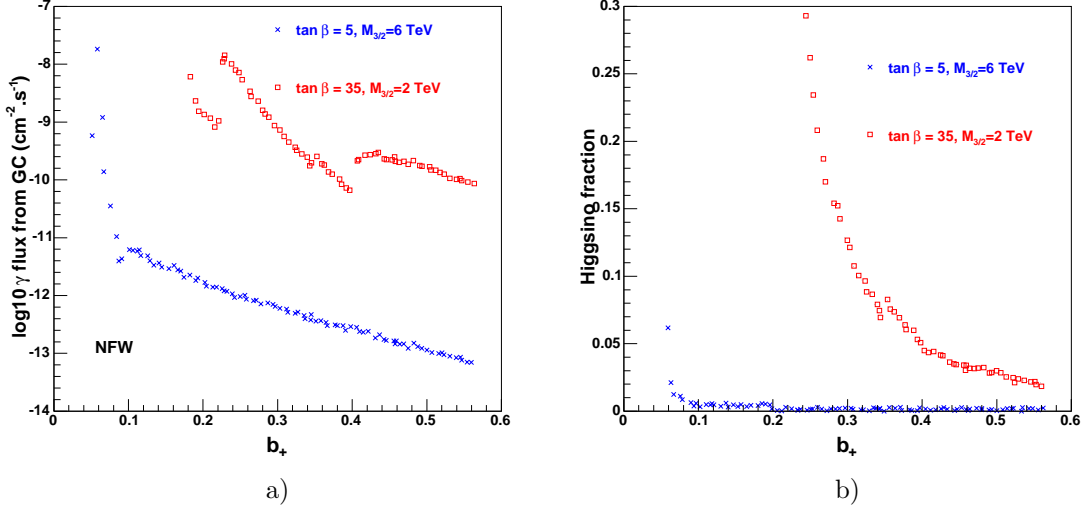
FIG. 7: Dilaton-dominated scenario. a) The integrated gamma flux ($E_\gamma > 1$ GeV) for a NFW profile in the dilaton parameter space as a function of the beta function b_+, for $t = 0.25$, $p = 0$, $\tan \beta = 5$ (blue crosses) and 35 (red boxes) and b) the neutralino higgsino fraction as a function of b_+ for the same values of $\tan \beta$. See the text for the comments.

- For a *fixed* value of $\tan \beta$ and a given profile density, the regions covered by the two models do not overlap. In other words, if we obtain the value of $\tan \beta$ by another experiment, the measurement of the gamma-ray flux will allow to distinguish or even exclude SUSY breaking scenarios.

- The flux is a decreasing function of the LSP mass, independently of the specific model adopted (see eq. 14): a heavier neutralino has a lower number density in the halo, and so a lower flux. Except some possible threshold effects, this is a general remark for any nature of indirect fluxes coming from neutralino annihilation at the Galactic Center. On the contrary, for lighter neutralino (dilaton–dominated scenario and mSugra) the threshold effect implies an increasing flux with m_χ. This effect is evaded for $m_\chi \gtrsim m_t$, when the $t\bar{t}$ channel is open.

- Fluxes in the dilaton breaking scenario are higher than in the moduli scenario (except for high $\tan\beta$ because of the A–pole contribution, see below). The highest flux in moduli dominated case is obtained for low $|\delta_{\rm GS}|$ (Fig. 5a), where the neutralino is completely wino but does not have a sufficient relic density to fulfill the dark matter content of the universe (see Fig.1). Those points are excluded by our cut on $\Omega > 0.03$. The remaining ones are situated in the near–zone "stau LSP" branch of Figs. 4 and 12.

In the dilaton dominated breaking scenario, most of the points are excluded at low m_χ because they do not respect the accelerator constraints on $m_{\chi_1^+}$ (and m_h), whereas heavy neutralinos are forbidden by the closed parameter space limited by the gaugino condensation group β–function coefficient b_+ ($b_+ \leq b_{E_8} \sim 0.57$). This parameter space is larger for lower values of $\tan\beta$ because barely constrained by the realization of the electroweak symmetry breaking condition ($\mu^2 > 0$). Most of the points with low integrated flux are excluded when imposing a higher limit on the relic density ($\Omega_\chi < 0.3$). This is due to the correlation between the fluxes and the relic density. In any case, if we take a lower upper omega limit (like the WMAP one) we keep the points with the best
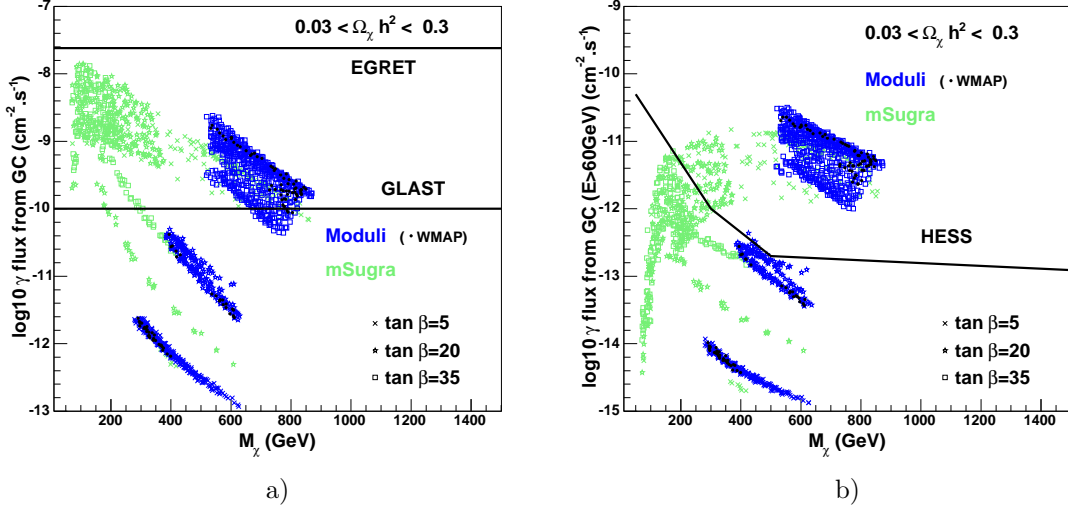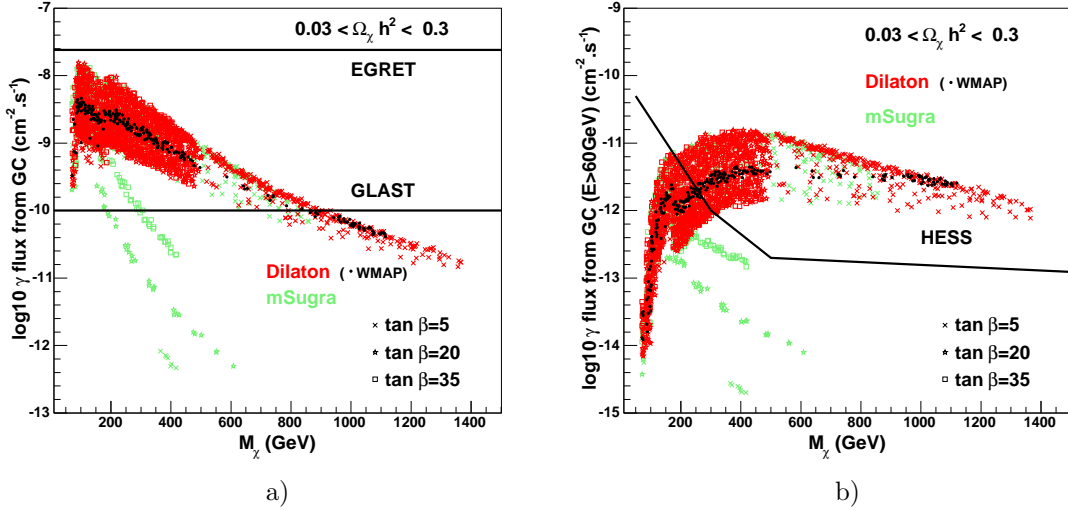
FIG. 8: **MODULI : The integrated flux of γ-ray** above 1 GeV in a) and 60 GeV in b) per centimeter square per second versus neutralino mass for $\tan\beta = 5, 20$ and 35 taking a NFW profile for the halo, after a scan in the moduli parameter space for $t = 0.25$, $p = 0$. The points that violate the accelerator constraints (see the appendix C for more details) are not represented here. Sensitivities of present and future experiments are represented in solid lines. We also show an "equivalent" mSUGRA cloud (see discussion in appendix B for the choice of parameter range).

FIG. 9: **DILATON : The integrated flux of γ-ray** above 1 GeV in a) and 60 GeV in b) per centimeter square per second versus neutralino mass for $\tan\beta = 5, 20$ and 35 taking a NFW profile for the halo, after a scan in the dilaton parameter space for $t = 0.25$, $p = 0$. The points that violate the accelerator constraints (see the appendix for more details) are not represented here. Sensitivities of present experiments and projects are represented in solid lines. We also show an "equivalent" mSUGRA cloud (see discussion in appendix for the choice of parameter space).

detection rates. As was pointed out in [19], the cosmologically favored region of the parameter space is similar to the Focus Point (FP) region present in mSUGRA [41], i.e. a mixed higgsino
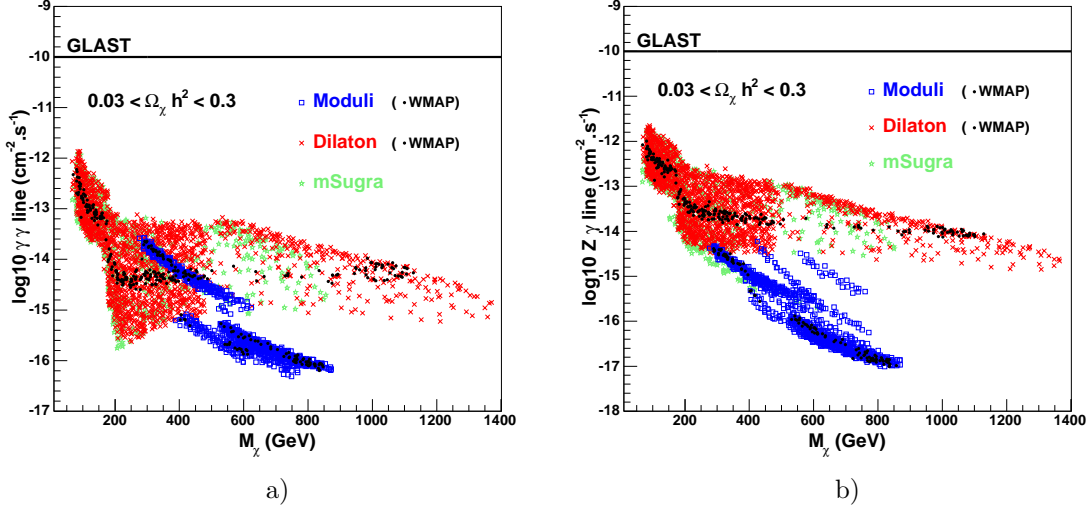
FIG. 10: **The $\gamma\gamma$ and $z\gamma$ lines** versus neutralino mass for $\tan\beta = 5, 20$ and 35 taking a NFW profile for the halo, after a scan in the dilaton parameter space and moduli one for $t = 0.25$, $p = 0$, and a comparison with mSugra. The points that violate the accelerator constraints are not represented here (see the appendix for the cut applied).

region leading to strong couplings and high gamma–ray fluxes dominated by $t\bar{t}$ (Z exchange) or WW (ZZ) final state processes. This explains the correlation between the dilaton and mSUGRA clouds on Fig. 9.

In the moduli dominated scenario, the dependence on $\tan\beta$ is not only due to the mass spectrum or a larger parameter space, but to the annihilation processes governing the gamma–ray fluxes. Indeed, in the moduli breaking scenario, one can have a relatively light pseudo scalar A. The annihilation of the neutralino is thus dominated by the s channel $\chi\chi \overset{A}{\to} b\bar{b}$ with a branching ratio approaching the 90 percents in most cases (the coupling $Ab\bar{b} \propto \tan\beta$, gives a factor 50 in σ between $\tan\beta = 5$ and 35). We can notice that thanks to the δ_{GS} parameter the A–pole can be obtained for lower value of $\tan\beta$ than in mSUGRA.

To study the observability of these fluxes, we have estimated the total gamma–ray flux above 60 GeV, and compared it with the predicted sensitivity of the HESS experiment (Figs. 8b and 9b). The low neutralino mass region (< 400 GeV)is not accessible to EGRET but will be explored by GLAST, whereas HESS will give more precise information for a heavy neutralino. In that sense, GLAST and HESS experiments are complementary. Indeed, evading the NFW profile assumption and taking a less cuspy density, the GLAST accessible region of our models is much less overlapping the HESS one. For instance, assuming a NFW profile, a non discovery of any signal in HESS *and* GLAST will exclude any dilaton dominated scenario and the high $\tan\beta$ regime of the moduli domination.

Finally, in the framework of effective heterotic models proposed in this paper, concerning direct and solar neutrino indirect detection, points satisfying all constraints in the dilaton case were all accessible to experiments whereas moduli was not [19]. Concerning gamma indirect detection, the conclusion depends strongly on the halo profile assumption. For a NFW shape, the dilaton model is still the most attractive for detection but the moduli one can also be tested by experiment. In that sense, gamma indirect detection is less an explicit test of SUSY breaking scenario but a very complementary way to give some hints on particles physics hypothesis and dark halo astrophysical assumptions.

We close this section by showing $\gamma\gamma$ and $Z\gamma$ line results on Figs. 10. Because dark mater in the halo is extremely non–relativistic, photons from these processes have an energy width of only $\Delta E_\gamma/E_\gamma \sim 10^{-3}$ and are effectively mono–energetic. While this signal would be the most spectacular of all possible indirect signals, as we can see in Figs. 10 the processes being loop-suppressed are much too low to be detected, even in any string scenario studied here. On another hand, the integrated flux explored before is more observable, but far less distinctive and will certainly require additional confirmation to unambiguously distinguish it from the background or other exotic sources.

V. SYNCHROTRON RADIATION

Another interesting source for the indirect search of DM in the Galactic halo is the detection of the neutralino via the synchrotron radiation created by the propagation of the $e^\pm$ products of neutralino annihilation, around the Galactic magnetic field. In our study, we have considered a magnetic field at equipartition at the Galactic center and constant elsewhere [38]

$$B(r) = \max \left[324\mu\mathrm{G} \left(\frac{r}{\mathrm{pc}} \right)^{-5/4}, 6\mu\mathrm{G} \right] \tag{16}$$

meaning that the field is constant for galacto-centric distances $r > 0.23$ pc.

Lower values of the magnetic field imply a shift of the synchrotron spectrum toward lower energies. As a consequence, the flux at low frequency will increase, favoring the detectability of our models. Nevertheless, we prefer to be conservative and consider a B field at equipartition.

The synchrotron flux per solid angle at a given frequency ν is given by [38]

$$L_\nu(\psi) \sim \frac{1}{4\pi} \frac{9}{8} \left(\frac{1}{0.29\pi} \frac{m_e^3 c^4}{e} \right)^{1/2} \frac{\sigma v}{M^2} Y_e(M, \nu) \nu^{1/2} I(\psi), \tag{17}$$

where

$$I(\psi) = \int_{line\ of\ sight} ds \rho^2(r(s, \psi)) B^{-1/2}(r(s, \psi)), \tag{18}$$

and s is the coordinate running along the line of sight. $Y_e(M, \nu)$ is the average number of secondary electrons above the energy $E_m(\nu)$ of the electron giving the maximum contribution at a given frequency ν and given magnetic field B. We recall that

$$E_m(\nu) = \left(\frac{4\pi}{3} \frac{m_e^3 c^4}{e} \frac{\nu}{B} \right)^{1/2} \tag{19}$$

In order to compare our predictions with the observational data, we to integrate over the corresponding solid angle, studying two distinct astrophysical situations and integrating over the string parameters of the theory in every case :

- Flux at $\nu = 408$ MHz in a cone of half width 4 arc sec pointing around the Galactic Center in a NFW halo model. The observed flux is ~ 0.05 Jy [52].

- Flux at $\nu = 327$ MHz in a cone of half width 13.5 arc sec pointing around the Galactic Center in a NFW halo model. The observed flux is ~ 362 Jy [53].
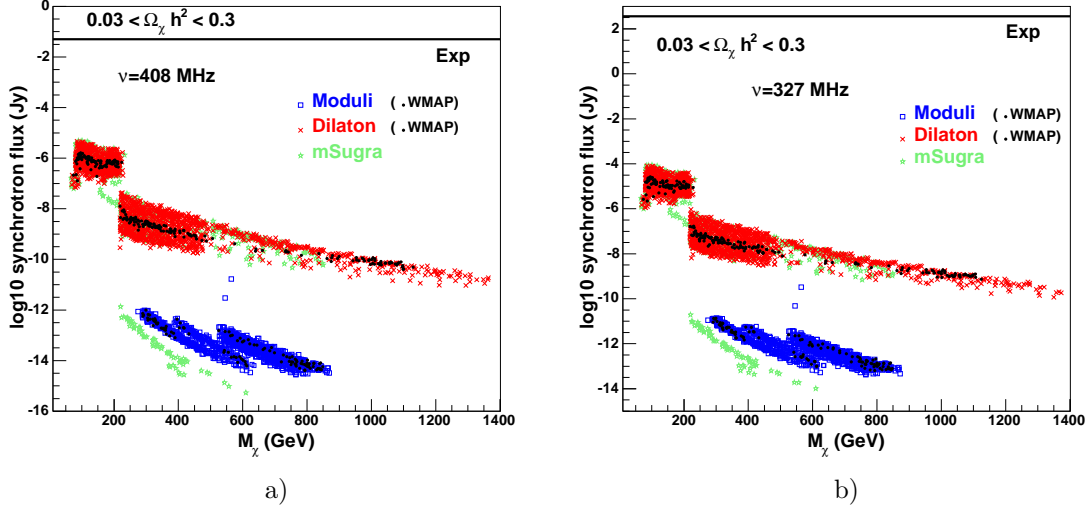
FIG. 11: **Predicted synchrotron radiation from the Galactic center** versus the neutralino mass for a NFW profile in a moduli dominated scenario and a dilaton one for $\tan\beta = 5, 20, 35$ (after experimental cuts) at a frequency of 408 MHz (left) and 327 MHz (right) compared to the flux observed limit at the same frequencies (horizontal lines). We also show the results of a "corresponding" mSugra scan

In our study, we have neglected two processes: self–absorption and absorption of electrons by the interstellar medium. In fact, it has been shown in Ref. [38] that in a NFW profile, the optical depth τ can be safely neglected unless very low frequencies are considered (of order ~ 1 Hz), which is not our case. Concerning the electron absorption, the authors of [38] observed that the absorption coefficient per length is such that $\alpha_\nu < 6 \ 10^{-16} pc^{-1}(B/\mu G)(\nu/GHz)^{-2}$, justifying our approximation.

In any case, for a NFW halo profile, the fluxes obtained for the models considered here do not constrain the mass of the DM particle, contrary to what happens in the case of Kaluza-Klein particles [38]. Naturally, the synchrotron flux shapes we obtain are similar to what we obtain for γ fluxes due to the same σv dependence, but the resulting values in the case of a NFW profile are several orders of magnitudes lower than experimental constraints. Recently, the calculation of synchrotron radiation from neutralino annihilation has been revisited [55]. Unfortunately the processes described there are not sufficient to make the flux in our models observable.

VI. CONCLUSIONS

We have studied gamma-ray and synchrotron emission from the Galactic center, in the context of an effective string inspired framework, and discussed two scenarios: in the first one, the SUSY breaking is transmitted by the compactification moduli T^α; while in second one, it is transmitted by the dilaton field S, via their respective auxiliary fields. Typically, models in the dilaton dominated SUSY breaking scenario lead to a higher annihilation rate than the moduli scenario. Concerning the continuum gamma-ray flux, both scenarios are within the reach of the experimental sensitivities of GLAST and HESS for a NFW halo profile. For the same profile, the gamma-ray line signal is suppressed and beyond the experimental sensitivity.

The synchrotron emission is too low to be constrained by experiments even with a more cuspy profile. Due to the dependence of the prospects of detection on both theoretical high energy physics

assumptions and astrophysical parameters of the halo dark matter distribution, gamma-ray indirect detection of neutralino dark matter can give interesting information either on astrophysical hypotheses or on the SUSY breaking scenario by the complementarity with other experimental searches like direct detection or neutrino telescopes (studied in [19] in the same context) or accelerators.

APPENDIX A: ANNIHILATION BRANCHING RATIOS FOR $\tan\beta = 5$.

We show here the figures corresponding to Fig.4 and 6 for $\tan\beta = 5$. The case of moduli domination regime is illustrated in Fig.12, while in Fig. 13 we show the case of dilaton dominated SUSY breaking.
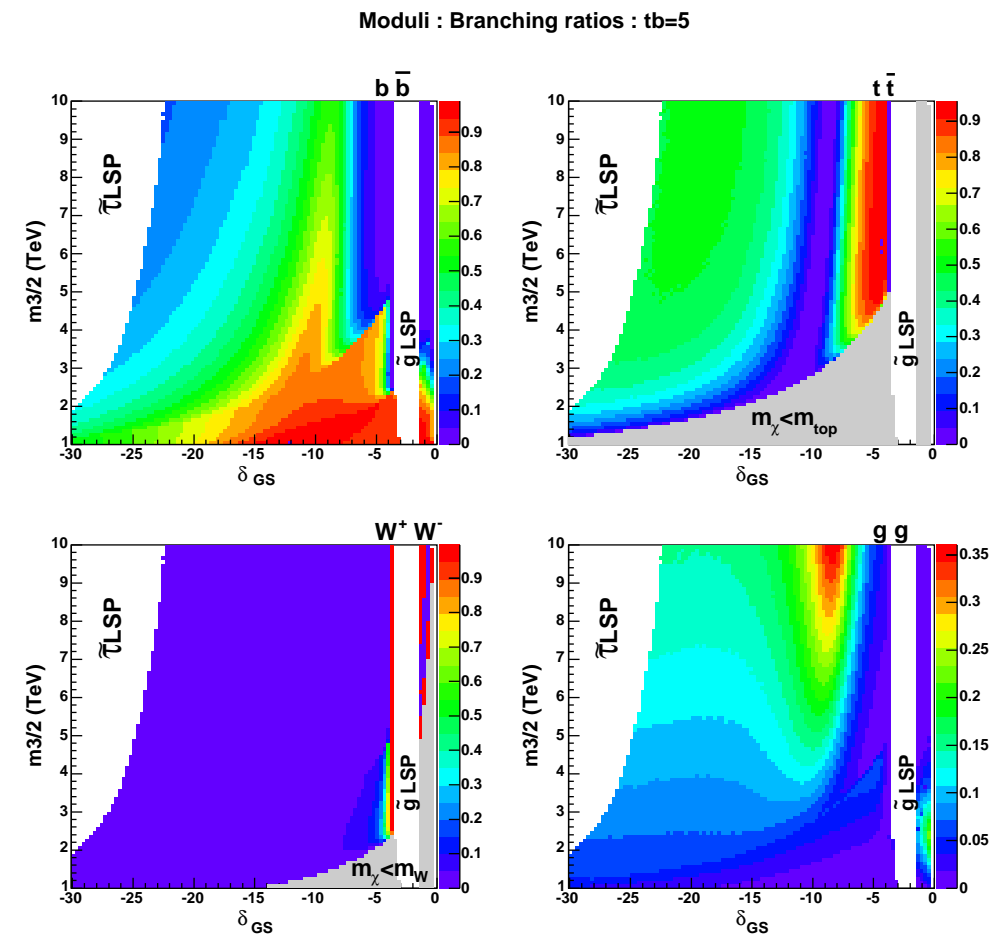

FIG. 12: Moduli domination regime: dominant annihilation branching ratios in the $(\delta_{GS}, m_{3/2})$ plane for $\tan\beta = 5$, $t = 0.25$, $p = 0$. Regions with gluino and stau LSP are indicated. We also show in grey the kinematically forbidden region for each channel.
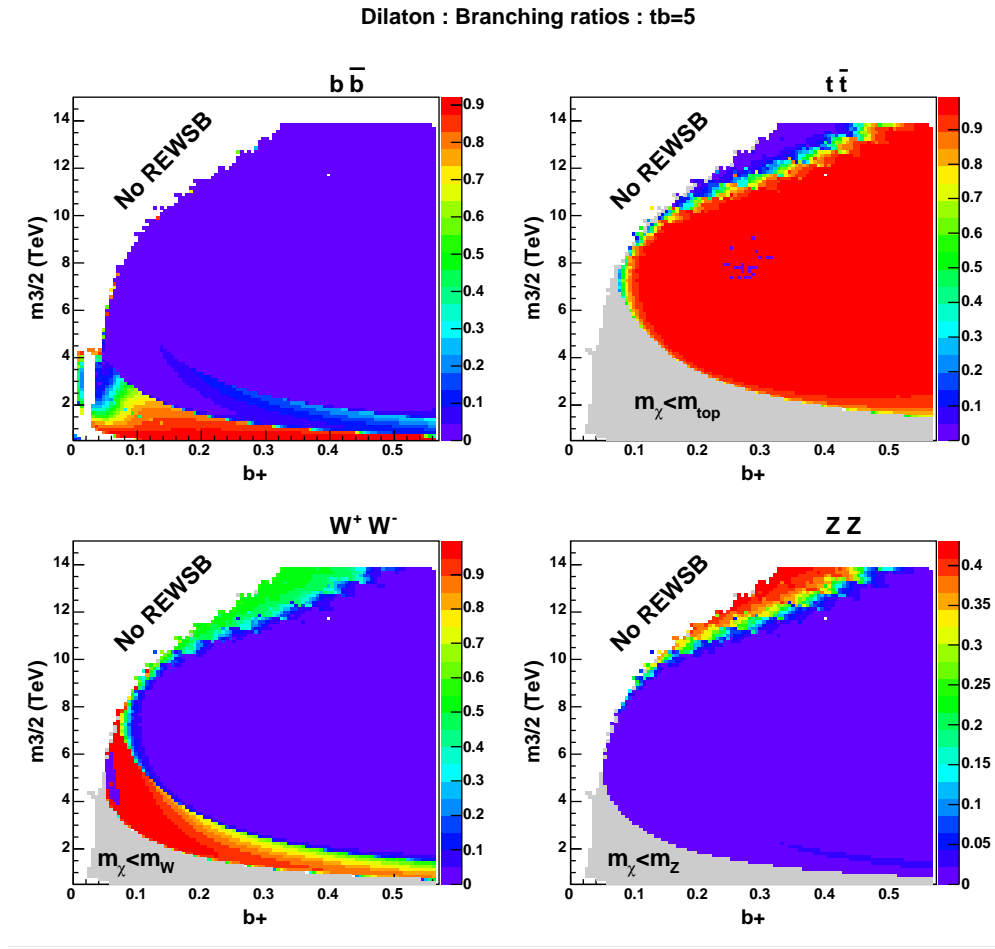
FIG. 13: Dominant annihilation branching ratios in the $(b_+, m_{3/2})$ plane for $\tan\beta = 5$, $t = 0.25$, $p = 0$. Regions where radiative electroweak symmetry breaking can not occur are indicated (No REWSB). We also show in grey the kinematically forbidden region for each channel.

APPENDIX B: PARAMETER RANGES

We performed a scan in the moduli and dilaton parameter space with the following values :

- Moduli :

  $t = 0.25, p = 0$

  $\tan\beta = 5$; $0 < m_{3/2} < 10000$ GeV ; $-30 < \delta_{GS} < 0$

  $\tan\beta = 20$; $0 < m_{3/2} < 16000$ GeV ; $-20 < \delta_{GS} < 0$

  $\tan\beta = 35$; $0 < m_{3/2} < 20000$ GeV ; $-10 < \delta_{GS} < 0$

- Dilaton:

  $t = 0.25, p = 0$

  $\tan\beta = 5$; $0 < m_{3/2} < 14000$ GeV ; $0 < b_+ < 0.57$

  $\tan\beta = 20$; $0 < m_{3/2} < 4500$ GeV ; $0 < b_+ < 0.57$

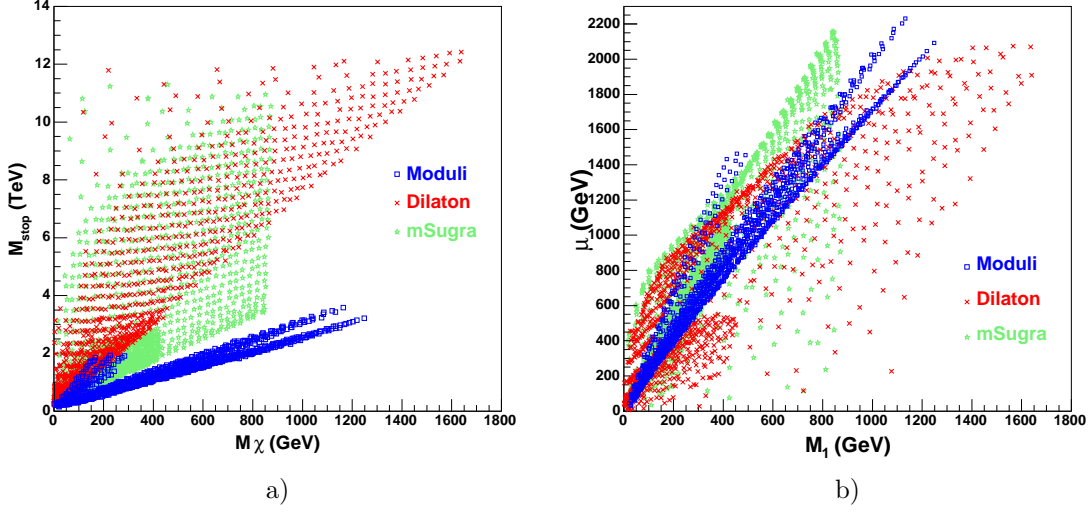 $\tan\beta = 35$; $0 < m_{3/2} < 4000$ GeV ; $0 < b_+ < 0.57$,

FIG. 14: Low energy $(m_\chi, m_{\tilde{t}})$ and (M_1, μ) planes showing that the parameter space we choose are quite equivalent.

corresponding to our previous study on direct detection and neutrino indirect detection [19]. We also show for comparison an equivalent mSugra cloud with the following parameter :

- mSugra :

  $A_0 = 0$

  $\tan \beta = 5$; $0 < m_0 < 14000$ GeV ; $0 < m_{1/2} < 2000$ GeV

  $\tan \beta = 20$; $0 < m_0 < 4000$ GeV ; $0 < m_{1/2} < 1500$ GeV

  $\tan \beta = 35$; $0 < m_0 < 3000$ GeV ; $0 < m_{1/2} < 1000$ GeV

We show on Fig. 14 two typical low energy planes: $(m_\chi, m_{\tilde{t}})$ and (M_1, μ) for $\tan \beta = 5, 35$ only. This illustrates that our choices of parameter ranges are coherent from the low energy point of view and allow for comparison between the different models. An extended study of such comparison is the subject of a forthcoming paper [42].

APPENDIX C: EXPERIMENTAL CONSTRAINTS

We apply the following conservative cuts on our models:

- Higgs mass: $m_h > 113.5$ GeV [43],

- Chargino mass: $m_{\chi^+} > 103.5$ GeV [44],

- Relic density: $0.03 < \Omega_\chi h^2 < 0.3$, but we also show the WMAP [26] range $\Omega_{\text{CDM}}^{WMAP} h^2 = 0.1126^{+0.0161}_{-0.0181}$,

- $b \to s\gamma$ Constraint [45]:
  $2.33 \times 10^{-4} < \text{BR}(b \to s\gamma) < 4.15 \times 10^{-4}$,

- The muon anomalous magnetic moment [46]: $-11.6 < \delta_\mu^{\text{new physics}} = \delta_\mu^{\text{exp}} - \delta_\mu^{\text{SM}} < 30.4$ [2 σ].

APPENDIX D: TOOLS

For our computations we have interfaced SUSPECT[47], MICROMEGAS[48] and DARKSUSY[49].

Concerning MSSM renormalization group equations and radiative electroweak symmetry breaking we use the code SUSPECT. It includes 2-loops RGE evolution from high scale down to low energy scale (we took $Q = \sqrt{\tilde{t}_1\tilde{t}_2}$ [50]) and minimizes the 1-loop scalar potential by solving iteratively the condition

$$\mu^2 = \frac{\left(m^2_{H_d} + \delta m^2_{H_d}\right) - \left(m^2_{H_u} + \delta m^2_{H_u}\right)\tan\beta}{\tan^2\beta - 1} - \frac{1}{2}M_Z^2, \tag{D1}$$

giving the μ parameter which drives the crucial neutralino higgsino fraction for dark matter studies.

We then transfer all MSSM parameters to the code MICROMEGAS which calculates the full physical mass spectrum including radiative corrections on Higgs masses and widths. The calculation of neutralino relic density is then achieved following the iterative procedure described in [51] and including all annihilation and co-annihilation processes by solving

$$\frac{dY}{dT} = \sqrt{\pi g_*(T)/45G}\langle\sigma v\rangle(Y^2 - Y_e^2 q) \tag{D2}$$

where Y is the abundance at the temperature T, g_* a degrees of freedom coming from thermodynamics, G the Newton constant and $\langle\sigma v\rangle$ the thermally average cross section of all processes concerning Y.

Masses and couplings are then entered in DARKSUSY which calculates the indirect detection rates of species $i = \gamma, e^+...$ coming from the Galactic Centre for a chosen galactic halo profile by splitting the particle physics dependance ($\propto \langle\sigma v\rangle d\phi/dE_i$, $\langle\sigma v\rangle$ including here only annihilations) and the astrophysics part $i.e$ the integration along the line of sight ($\int ds\rho^2(r(s,\psi))$, $\rho(r)$ being the dark matter density distribution).

[1] G. Bertone, D. Hooper and J. Silk, arXiv:hep-ph/0404175.
[2] J. R. Ellis, T. Falk, G. Ganis, K. A. Olive and M. Srednicki, *Phys. Lett.* **B510** (2001) 236;
    J. R. Ellis, K. A. Olive and Y. Santoso, *New Jour. Phys.* **4** (2002) 32;
    L. Roszkowski, R. Ruiz de Austri and T. Nihei, *JHEP* **0108** (2001) 024;
    A. Djouadi, M. Drees and J. L. Kneur, *JHEP* **0108** (2001) 055;
    H. Baer, C. Balazs and A. Belyaev, *JHEP* **0203** (2002) 042.
    U. Chattopadhyay, A. Corsetti and P. Nath, *Phys. Rev.* D **68**, 035005 (2003).
    H. Baer, A. Belyaev, T. Krupovnickas and J. O'Farrill, arXiv:hep-ph/0405210.
[3] J. R. Ellis, A. Ferstl, K. A. Olive and Y. Santoso, *Phys. Rev.* D **67**, 123502 (2003)
[4] V. Berezinsky, A. Bottino, J. Ellis, N. Fornengo, G. Mignola, S. Scopel, *Astropart.Phys.* **5** (1996) 1-26, arXiv:hep-ph/9508249.
[5] P. Nath, R. Arnowitt, *Phys.Rev.* **D56** (1997) 2820-2832, arXiv:hep-ph/9701301.
[6] V. Bertin, E. Nezri, J. Orloff, *JHEP* **02** (2003) 046, arXiv:hep-ph/0210034.
[7] A. Birkedal-Hansen B. D. Nelson *Phys.Rev.* **D67** (2003) 095006, arXiv:hep-ph/0211071.
[8] A. Corsetti, P. Nath, *Phys.Rev* **D64** (2001) 125010, arXiv:hep-ph/0003186.
[9] S. Profumo, Phys. Rev. D **68**, 015006 (2003)
[10] P. Ullio, Nucl. Phys. Proc. Suppl. **110**, 82 (2002).
[11] A. Cesarini, F. Fucito, A. Lionetto, A. Morselli and P. Ullio, arXiv:astro-ph/0305075.

[12] D. Hooper and L. T. Wang, Phys. Rev. D **69**, 035001 (2004) [arXiv:hep-ph/0309036].

[13] A. Bottino, F. Donato, N. Fornengo and S. Scopel, arXiv:hep-ph/0401186.

[14] D. G. Cerdeno and C. Munoz, arXiv:hep-ph/0405057.

[15] U. Chattopadhyay and P. Nath, arXiv:hep-ph/0405157.

[16] S. Profumo and P. Ullio, arXiv:hep-ph/0406018.

[17] P. Binétruy, M. K. Gaillard and B. D. Nelson, *Nucl. Phys.* **B604** (2001) 32.

[18] P. Binétruy, A. Birkedal-Hansen, Y. Mambrini, B.D. Nelson arXiv:hep-ph/0308047.

[19] P. Binétruy, Y. Mambrini, E. Nezri arXiv:hep-ph/0312155.

[20] G.L. Kane, J. Lykken, S. Mrenna, B.D. Nelson, L.T. Wang, T.T. Wang *Phys.Rev.* **D67** (2003) 045008 arXiv:hep-ph/0209061.

[21] P. Binétruy, M. K. Gaillard and Y.-Y. Wu, *Nucl. Phys.* **B481** (1996) 109.

[22] P. Binétruy, M. K. Gaillard and Y.-Y. Wu, *Nucl. Phys.* **B493** (1997) 27.

[23] M. K. Gaillard, B. D. Nelson and Y.-Y. Wu, *Phys. Lett.* **B459** (1999) 549.

[24] M. K. Gaillard and B. D. Nelson, *Nucl. Phys.* **B588** (2000) 197.

[25] ALEPH collaboration*Phys.Lett.* **B583** (2004) 247-263

[26] C. L. Bennett *et al.*, *Astrophys.J.Suppl.* 148:1,2003
    D. N. Spergel *et al.*, *Astrophys.J.Suppl.* 148:175,2003

[27] J. F. Navarro, C. S. Frenk and S. D. M. White, Astrophys. J. **490** (1997) 493.

[28] A. V. Kravtsov, A. A. Klypin, J. S. Bullock and J. R. Primack, arXiv:astro-ph/9708176.

[29] B. Moore, T. Quinn, F. Governato, J. Stadel and G. Lake, Mon. Not. Roy. Astron. Soc. **310** (1999) 1147 [arXiv:astro-ph/9903164].

[30] L. Bergstrom, P. Ullio and J. H. Buckley, Astropart. Phys. **9** (1998) 137 [arXiv:astro-ph/9712318].

[31] R. Schödel et al. Nature 419, 694 (2002)

[32] P. Gondolo and J. Silk, Phys. Rev. Lett. **83** (1999) 1719 [arXiv:astro-ph/9906391].

[33] G. Bertone, G. Sigl and J. Silk, Mon. Not. Roy. Astron. Soc. **337** (2002) 98 [arXiv:astro-ph/0203488].

[34] de Blok, W. J. G., McGaugh, S. S., Bosma, A., and Rubin, V. C., ApJ 552, L23

[35] R. A. Swaters, B. F. Madore, F. C. V. Bosch and M. Balcells, Astrophys. J. **583** (2003) 732 [arXiv:astro-ph/0210152].

[36] F. C. van den Bosch, B. E. Robertson, J. J. Dalcanton and W. J. G. de Blok, arXiv:astro-ph/9911372.

[37] E. Hayashi *et al.*, arXiv:astro-ph/0310576.

[38] G. Bertone, G. Servant and G. Sigl, Phys. Rev. D **68** (2003) 044008 [arXiv:hep-ph/0211342].

[39] G. Jungman, M. Kamionkowski and K. Griest, Phys. Rept. 267 (1996) 195.

[40] S. W. Barwick *et al.* [HEAT Collaboration], Astrophys. J. **482**, L191 (1997) [arXiv:astro-ph/9703192].

[41] J.L. Feng, K.T. Matchev, F. Wilczek, *Phys.Rev.* **D63** (2001) 045024, arXiv:astro-ph/0008115.

[42] P. Binétruy, Y. Mambrini, E. Nezri in preparation.

[43] ALEPH Collaboration (A. Heister et al.) *Phys.Lett.* **B526** (2002) 191.

[44] ALEPH Collaboration (A. Heister et al.) *Phys.Lett.* **B533** (2002) 223.

[45] M. Battaglia, A. De Roeck, J. Ellis, F. Gianotti, K. T. Matchev K. A. Olive, L. Pape, G. Wilson, *Eur. Phys. J.* **C22** (2001) 535.

[46] M. Davier, S. Eidelman, A. Hocker and Z. Zhang, Eur. Phys. J. C **31** (2003) 503 [arXiv:hep-ph/0308213].

[47] A. Djouadi, J. L. Kneur and G. Moultaka, *SuSpect: a Fortran Code for the Supersymmetric and Higgs Particle Spectrum in the MSSM*, hep-ph/0211331, http://www.lpm.univ-montp2.fr:6714/~kneur/suspect.html.

[48] G. Belanger, F. Boudjema, A. Pukhov and A. Semenov, *MicrOMEGAs: A Program for Calculating the Relic Density in the MSSM*, *Comput.Phys.Commun.* **149** (2002) 103-120, hep-ph/0112278, http://wwwlapp.in2p3.fr/lapth/micromegas.

[49] P. Gondolo, J. Edsjo, P. Ullio, L. Bergstrom, M. Schelke and E. A. Baltz, *DarkSUSY: A numerical package for supersymmetric dark matter calculations*,astro-ph/0211238. P. Gondolo, J. Edsjo, L. Bergstrom, P. Ullio, et T. Baltz, *DarkSusy program, http://www.physto.se~edsjo/darksusy/*

[50] G. Gamberini, G. Ridolfi and F. Zwirner, *Nucl. Phys.* **B331** (1990) 331.

[51] P. Gondolo and G. Gelmini, Nucl. Phys. B **360** (1991) 145.

[52] R. D. Davies, D. Walsh and R. S. Booth, *Mon. Not. Roy. Astron. Soc.* , **177** (1976) 319

[53] T. N. La Rosa, N. E. Kassim, T. J. Lazio and S. D. Hyman, *Astron. Journ.* , **119** (2000) 207

[54] L. Bergstrom, P. Ullio and J. H. Buckley, "Observability of gamma rays from dark matter neutralino annihilations in the Milky Way halo,", *Astropart. Phys.* , **9** (1998) 137 [astro–ph/9712318].

[55] R. Aloisio, P. Blasi and A. V. Olinto, arXiv:astro-ph/0402588.

[56] For simplicity, we assume here that $M_{\mathrm{STR}} \sim \mu_{\mathrm{UV}} \sim \mu_R \sim M_{\mathrm{GUT}}$ (the corresponding error is logarithmic and appears in a loop factor).

[57] We can compute the analytical expression of δ_{GS} where this change of nature appears by solving in Eq. 6 $M_1^{GUT} = 2M_2^{GUT}$ ($M_1^{LOW} = M_2^{LOW}$) that gives $\delta_{GS} = -\frac{46}{15} \sim -3$.

[58] We are in the so called decoupling regime.